

# Shubnikov-de Haas oscillations spectrum of the strongly correlated quasi-2D organic metal $(\text{ET})_8[\text{Hg}_4\text{Cl}_{12}(\text{C}_6\text{H}_5\text{Br})]_2$ under pressure.

David Vignolles<sup>1</sup>, Alain Audouard<sup>1</sup>, Rustem B. Lyubovskii<sup>2</sup>, Marc Nardone<sup>1</sup>, Enric Canadell<sup>3</sup>, Elena I. Zhilyaeva<sup>2</sup>, and Rimma N. Lyubovskaya<sup>2</sup>

<sup>1</sup> Laboratoire National des Champs Magnétiques Pulsés <sup>a</sup>, 143 avenue de Rangueil, 31400 Toulouse, France.

<sup>2</sup> Institute of Problems of Chemical Physics, RAS, 142432 Chernogolovka, MD, Russia.

<sup>3</sup> Institut de Ciència de Materials de Barcelona, CSIC, Campus de la UAB, 08193, Bellaterra, Spain.

Received: December 1, 2008/ Revised version: date

**Abstract.** Pressure dependence of the Shubnikov-de Haas (SdH) oscillations spectra of the quasi-two dimensional organic metal  $(\text{ET})_8[\text{Hg}_4\text{Cl}_{12}(\text{C}_6\text{H}_5\text{Br})]_2$  have been studied up to 1.1 GPa in pulsed magnetic fields of up to 54 T. According to band structure calculations, its Fermi surface can be regarded as a network of compensated orbits. The SdH spectra exhibit many Fourier components typical of such a network, most of them being forbidden in the framework of the semiclassical model. Their amplitude remains large in all the pressure range studied which likely rules out chemical potential oscillation as a dominant contribution to their origin, in agreement with recent calculations relevant to compensated Fermi liquids. In addition to a strong decrease of the magnetic breakdown field and effective masses, the latter being likely due to a reduction of the strength of electron correlations, a sizeable increase of the scattering rate is observed as the applied pressure increases. This latter point, which is at variance with data of most charge transfer salts is discussed in connection with pressure-induced features of the temperature dependence of the zero-field interlayer resistance.

**PACS.** 71.18.+y Fermi surface: calculations and measurements; effective mass, g factor – 71.20.Rv Polymers and organic compounds – 72.15.Gd Galvanomagnetic and other magnetotransport effects

## 1 Introduction

Quantum oscillations spectra of quasi-two-dimensional (q-2D) multiband metals are known to contain many Fourier components. In addition to those that can be attributed to closed orbits, eventually induced by magnetic breakdown (MB), linear combinations of few basic frequencies that are not predicted by the semiclassical model [1, 2] can nevertheless be observed. This frequency mixing phenomenon can be linked to both the q-2D nature of the dispersion relation which is liable to give rise to a field-dependent oscillation of the chemical potential [3] and to the Fermi surface (FS) topology that can be regarded as a network of orbits coupled by MB [4]. Despite both theoretical and experimental efforts, the latter being mainly focused on organic metals based on the ET molecule (where ET stands for bisethylenedithia-tetrathiofulvalene) with the FS originating from the hybridization of one orbit with an area equal to that of the first Brillouin zone (FBZ), quantitative interpretation of the data is still an open problem.

Networks of orbits can also result from the hybridization of two or more pairs of q-1D sheets as it is the case of the room temperature FS of numerous oxide bronzes. However hidden nesting properties [5] lead to the condensation of a charge density wave which strongly modifies the FS at low temperature in most cases. As a result, quantum oscillations spectra observed e. g. in monophosphate tungsten bronzes [6] can hardly be reconciled with band

structure calculations [7]. Analogous problematic can be observed in the q-2D organic metal  $\beta''$ -(ET)(TCNQ) [8].

On the contrary, although the FS of the q-2D charge transfer salt  $(\text{ET})_8\text{Hg}_4\text{Cl}_{12}(\text{C}_6\text{H}_5\text{Cl})$ , noted hereafter as (Cl, Cl), originates from the hybridization of two pairs of q-1D sheets as well, it remains metallic down to the lowest temperatures. According to band structure calculations [9], its FS is composed of two compensated orbits labelled  $a$  in the following with an area of 13 % of the FBZ area. Shubnikov-de Haas (SdH) oscillations spectra of this compound [10], which otherwise exhibit many frequency combinations, as discussed below, are in good agreement with this picture since the main Fourier component has a frequency  $F_a = 241.5 \pm 2$  T that corresponds to 11 % of the FBZ area. This is also the case of the isostructural compound  $(\text{ET})_8[\text{Hg}_4\text{Cl}_{12}(\text{C}_6\text{H}_5\text{Br})]_2$ , noted hereafter as (Cl, Br), which has been even more extensively studied at high magnetic field [11, 12] although its FS has not been reported up to now.

With respect to the interpretation of frequency combinations, applied pressure can be useful in order to tune both the transverse interactions (which are involved in the chemical potential oscillations) [13] and the MB gaps. In a first step, band structure calculations of the (Cl, Br) compound at ambient pressure are reported which confirm that its FS can be regarded as a network of compensated orbits. In a second step, the temperature dependence of the interlayer resistance under pressure is considered. Finally, the pressure-induced change of the SdH oscillations

<sup>a</sup> UMR 5147: Unité Mixte de Recherche CNRS - Université

spectrum, MB field, effective masses and scattering rate is investigated up to 1.1 GPa.

## 2 Experimental

The studied crystals were prepared by the electrochemical method reported in [14]. Tight binding band structure calculations, based on X-ray data collected at room temperature and ambient pressure, were performed using the same method as reported in [9]. The calculations use an extended Hückel effective one-electron Hamiltonian [15]. The off-diagonal matrix elements of the Hamiltonian were calculated according to the modified Wolfsberg-Helmholz formula [16]. All valence electrons were explicitly taken into account in the calculations and the basis set consisted of double- $\zeta$  Slater-type orbitals for all atoms, except hydrogen.

Interlayer zero-field resistance and magnetoresistance measurements were performed on crystals with approximate dimensions  $0.5 \times 0.5 \times 0.1 \text{ mm}^3$ . Electrical contacts to the crystal were made using annealed platinum wires of  $20 \text{ }\mu\text{m}$  in diameter glued with graphite paste. Alternating current ( $1 \text{ }\mu\text{A}$ ,  $77 \text{ Hz}$ ) and ( $5$  to  $10 \text{ }\mu\text{A}$ ,  $20 \text{ kHz}$ ) was injected parallel to the  $a^*$  direction for measurements of the interlayer zero-field resistance and magnetoresistance, respectively. Hydrostatic pressure was applied up to 1.1 GPa in an anvil cell designed for isothermal measurements in pulsed magnetic fields [17]. In the following, the pressure applied at room temperature is considered although a slight crystal size-dependent pressure loss on cooling cannot be excluded [18]. Magnetoresistance ex-

periments were performed up to 54 T in pulsed magnetic field with pulse decay duration of 0.36 s, in the temperature range from 1.5 K to 4.2 K. Magnetic field was applied normal to the conducting ( $bc$ ) plane. A lock-in amplifier with a time constant of  $30 \text{ }\mu\text{s}$  was used to detect the signal across the potential contacts. Analysis of the oscillatory magnetoresistance is based on discrete Fourier transforms of the data, calculated with a Blackman window.

## 3 Results and discussion

The band structure calculations and FS of the (Cl, Br) compound displayed in Fig. 1 are based on crystallographic data recorded at ambient pressure and room temperature. The repeat unit of the donor layer contains 8 ET molecules so that the band structure of Fig. 1a contains 8 bands mainly based on the highest occupied molecular orbitals of ET. With the usual oxidation states of  $\text{Cl}^-$  and  $\text{Hg}^{2+}$ , the average charge of the ET donors is  $+1/2$ . Consequently, two bands in Fig. 1a should be formally empty. Since the second and third bands from the top overlap, the system must be metallic and its FS must contain both electron and hole contributions with the same area. More precisely, as it is the case for (Cl, Cl) [9], the FS (see Fig. 1b) originates from two pairs of crossing q-1D sheets and constitutes a network of compensated electron (around M) and hole (around Z) closed orbits elongated along the  $(b^* + c^*)$  and  $c^*$  directions, respectively. These orbits are both labelled  $a$  hereafter since they have the same area. Both the band structure and FS of Fig. 1 are very similar to those previously reported for the (Cl, Cl) compound [9].

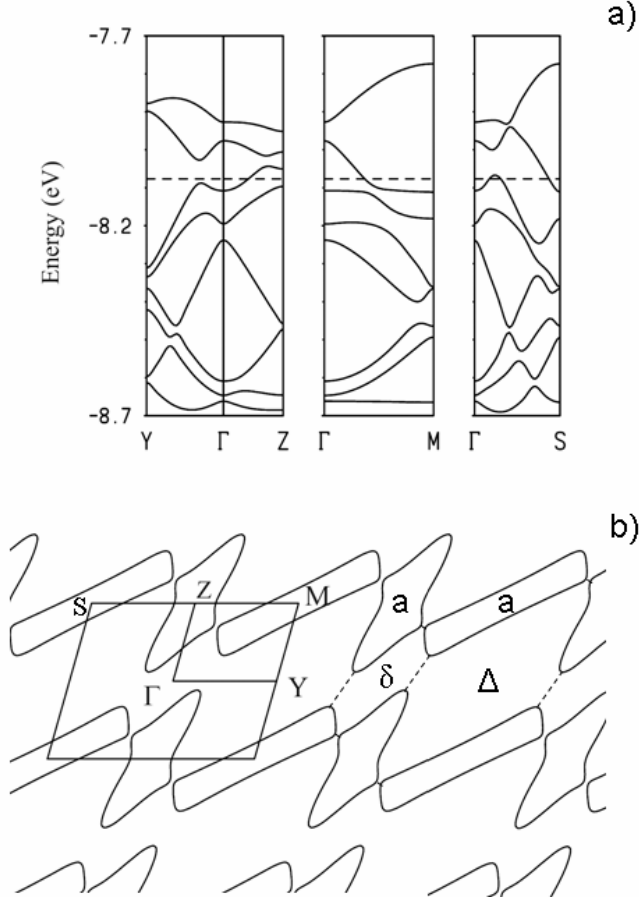


**Fig. 1.** (a) Dispersion relations at ambient pressure of  $(\text{ET})_8[\text{Hg}_4\text{Cl}_{12}(\text{C}_6\text{H}_5\text{Br})]_2$ . The dashed lines marks the Fermi level. (b) Fermi surface (FS) corresponding to (a).  $\Gamma$ , Y, Z, S and M refer to  $(0, 0)$ ,  $(b^*/2, 0)$ ,  $(0, c^*/2)$ ,  $(-b^*/2, c^*/2)$  and  $(b^*/2, c^*/2)$ , respectively. Labels  $a$ ,  $\delta$  and  $\Delta$  correspond to the FS pieces discussed in the text.

For instance whereas the area of the closed orbits of the (Cl, Br) compound is 16.1 % of the FBZ area, according to data in Fig. 1, calculations for (Cl, Cl) using the same computational details as in the present case lead to an area of 16.7 % of the FBZ area. Although this is not surprising since the two compounds are isostructural, these results justify a posteriori the previous data analysis based on a

FS topology analogous to that of the (Cl, Cl) compound [11,12,19]. Let us note that similar calculations led to a more substantial variation of the orbits area for the (Br, Cl) compound (9.6 % of the FBZ area). This suggests that replacement of Br by Cl in the anion layer has a considerably stronger effect on the FS than the same replacement in the solvent molecules. The small difference in orbits area between the (Cl, Br) and (Cl, Cl) compounds is in agreement with the experimental results. Nevertheless, a slight discrepancy between calculations and quantum oscillations spectra can be observed since the closed orbits area of (Cl, Br) amounts to 16.1 % and 11 % of the FBZ area in the former and latter cases, respectively.

Zero-field interlayer resistance and magnetotransport were studied on three crystals. Since they yield consistent results, we concentrate on the most extensively studied one in the following. It should be noted that all the features reported hereafter are reversible as the pressure is released.

Temperature dependence of the zero-field interlayer resistance at various applied pressures is displayed in Fig. 2. The room temperature resistance decreases as the pressure increases ( $d\ln R/dP = -1 \text{ GPa}^{-1}$ ) while the low temperature value remains almost unaffected. As a result, the residual resistivity ratio (RRR) decreases monotonously by about a factor of 3 as the pressure increases up to 1.1 GPa. Whereas the resistance continuously decreases as the temperature decreases at ambient pressure, a resistance maximum is observed under pressure, the amplitude of which is maximum around 0.5 GPa. Data under pres-

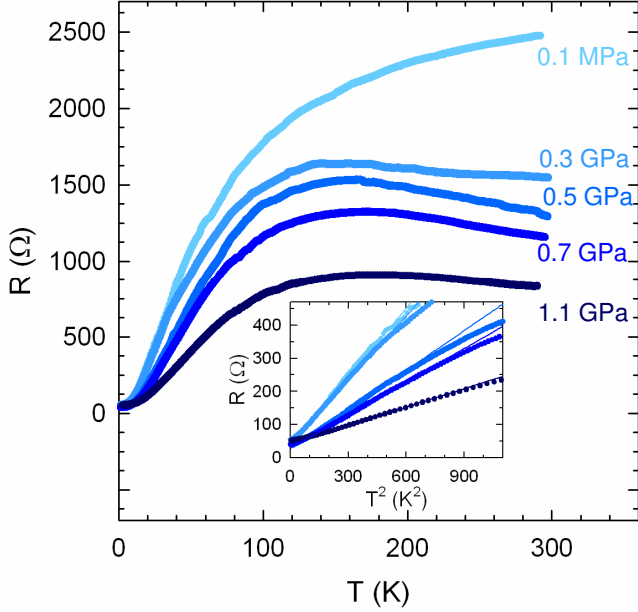


**Fig. 2.** (color on line) Temperature dependence of the zero-field interlayer resistance at various applied pressures. The low temperature part of the data is plotted as a function of  $T^2$  in the inset.

sure share similarities with the sample-dependent zero-field interlayer resistance of the high-resistance variant of  $\kappa$ -(ET)<sub>2</sub>Cu[N(CN)<sub>2</sub>]Br whose resistance increases as the temperature decreases down to about 100 K and strongly decreases at lower temperatures [20]. A similar temperature dependence is also observed for other charge transfer salts such as  $\kappa$ -(ET)<sub>2</sub>Cu(NCS)<sub>2</sub> [21] or  $\kappa$ -(ET)<sub>2</sub>Cu[N(CN)<sub>2</sub>]Cl [22]. As reported in Ref. [23], the resistance maximum observed in  $\kappa$ -(ET)<sub>2</sub>Cu[N(CN)<sub>2</sub>]Br is certainly related to disorder and possibly to point defects. Indeed, due to a decrease of the Dingle temperature, the SdH oscillations amplitude increases as the amplitude of the resistance maximum decreases. It should be noted that the effect of pressure on the zero-field transport properties of this

compound is at variance with that of Fig. 2 since the amplitude of the resistance maximum decreases continuously as the applied pressure increases in the former case. In other words, data in zero-field could suggest that, even though the scattering rate in  $\kappa$ -(ET)<sub>2</sub>Cu[N(CN)<sub>2</sub>]Br decreases under pressure, it increases in the case of the (Cl, Br) compound, at least up to 0.5 GPa. Oppositely, X-ray irradiation of  $\kappa$ -(ET)<sub>2</sub>Cu(NCS)<sub>2</sub> lead to a decrease of the resistance maximum amplitude [24]. However, as far as  $\kappa$ -(ET)<sub>2</sub>Cu[N(CN)<sub>2</sub>]Cl is concerned, this behaviour is due to a significant irradiation-induced increase of the carrier concentration [25] that cannot hold in our case.

It should be also mentioned that a coherent-incoherent crossover of small polarons, driven by the strength of the electron-phonon coupling, can also lead to interlayer resistance maximum [26,27]. Alternatively, electron correlations have been invoked in order to account for such resistance behaviour [22,28]. As a matter of fact, a  $T^2$  variation of the resistance ( $R = R_0 + AT^2$ ) is observed at low temperature (see the inset of Fig. 2). Owing to the crystal dimensions,  $A$  ranges from  $\sim 0.2 \text{ } \Omega\text{cmK}^{-2}$  at ambient pressure to  $\sim 0.05 \text{ } \Omega\text{cmK}^{-2}$  at 1.1 GPa. Such a behaviour which is commonly observed both in charge transfer salts [20,22] and inorganic low dimensional compounds such as Sr<sub>2</sub>RuO<sub>4</sub> [29] is currently regarded as the signature of a strongly correlated Fermi liquid. This latter point and the above statement regarding the pressure dependence of the scattering rate are further discussed at the light of the magnetoresistance data reported hereafter.

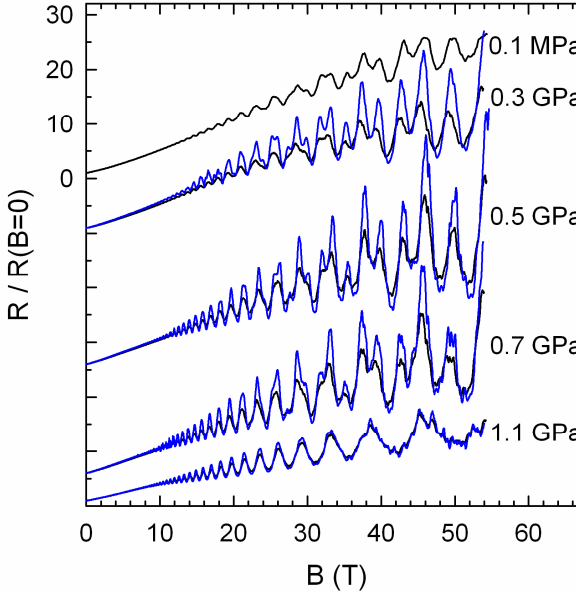


**Fig. 3.** (color on line) Field-dependent interlayer resist at various applied pressures. Curves have been shifted by an arbitrary amount for clarity. Black and blue solid correspond to data measured at 4.2 K and 1.7 K, respect

Fourier analysis of interlayer magnetoresistance (few examples of which are given in Fig. 3) are disp in Fig. 4. As previously reported for ambient pressure [11], many frequencies are observed in all the exp pressure range. Most of them are linear combinatic that linked to the compensated electron- and hole orbits (labelled  $a$  in Fig. 1) and of the FS pieces locaueu in-between (labelled  $\delta$  and  $\Delta$  in Fig. 1). These two latter FS pieces correspond to so called "forbidden orbits"<sup>1</sup> as it is the case of most of the observed frequency combinations. Oppositely, the Fourier component  $2a + \delta$  corre-

<sup>1</sup> As reported in Ref. [11], these FS pieces could correspond to MB-induced closed orbits or QI paths. However, the corresponding effective mass and MB damping factor would be much too large and small, respectively, to account for the data

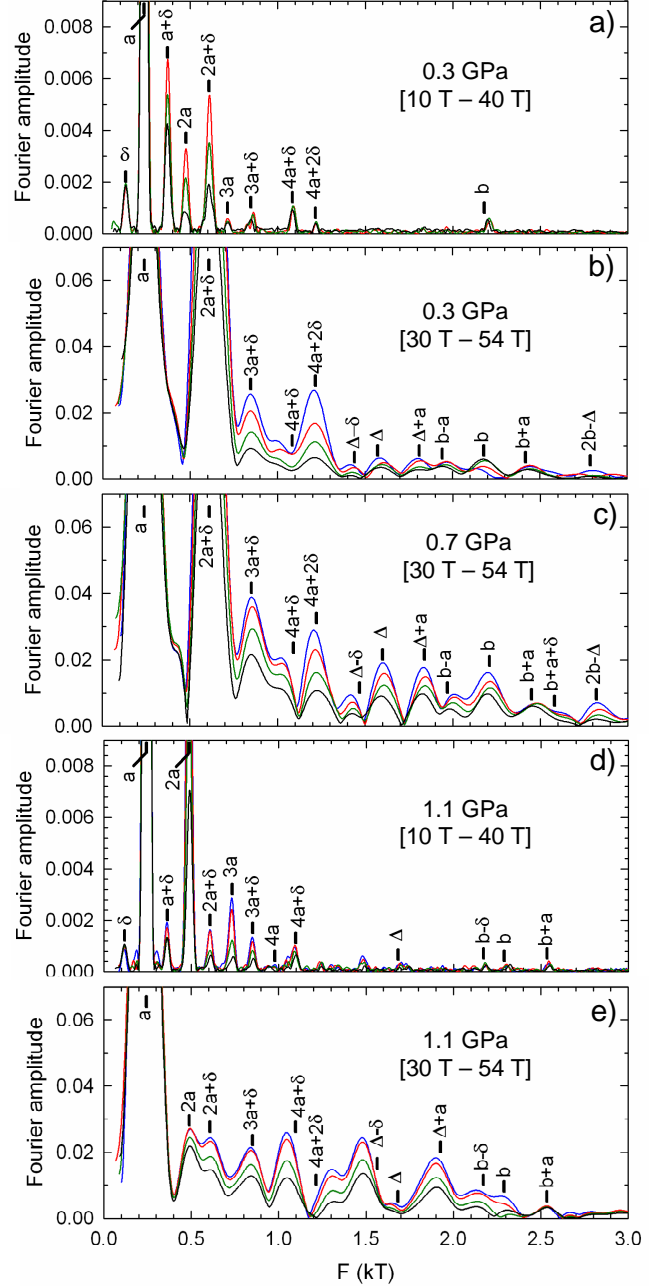


**Fig. 4.** (color on line) Fourier analysis of the oscillatory part of the magnetoresistance at various applied pressures and field ranges. Blue, red, green and black solid lines correspond to data at 1.7, 2.5, 3.4 and 4.2 K, respectively. Black vertical lines are marks calculated with the set of frequency values ( $F_a$ ,  $F_\delta$  and  $F_\Delta$ ) that best fits to the Fourier spectra.

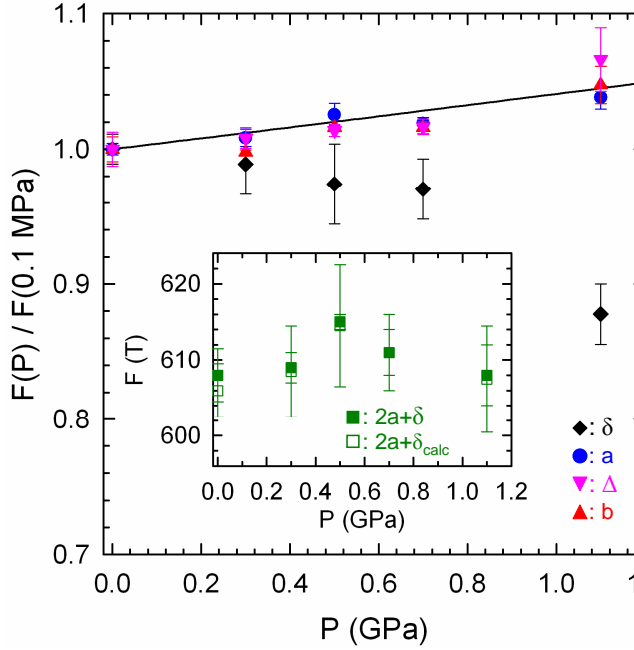


**Fig. 5.** (color on line) Pressure dependence of the normalized frequency of the Fourier components  $\delta$ ,  $a$ ,  $\Delta$  and  $b$  deduced from data in Fig. 4). The ambient pressure values are  $F_\delta = 600$  T,  $F_a = 235.5$  T and  $F_\Delta = 1577$  T [11]. The inset displays the pressure dependence of  $F_{2a+\delta}$ . Open squares stand for values calculated as  $F_{2a+\delta} = 2F_a + F_\delta$ .

sponds to a MB orbit while the  $b$  frequency corresponds to QI paths involving an area equal to that of the FBZ ( $F_b = 2F_a + F_\delta + F_\Delta$ ) [10,11]. At high field and (or) high pressure, shift of few frequency combinations (such as  $4a + \delta$  or  $\Delta - \delta$ ) that could as well correspond to additional frequencies can be observed in Figs. 4(b) - (e). Although more data is needed in order to discuss the origin of these latter features, it can be inferred that they could arise from slight change of the FS. Nevertheless, most of the observed Fourier components remain linear combinations of the three basic frequencies reported above which allows for the study of their pressure dependence.

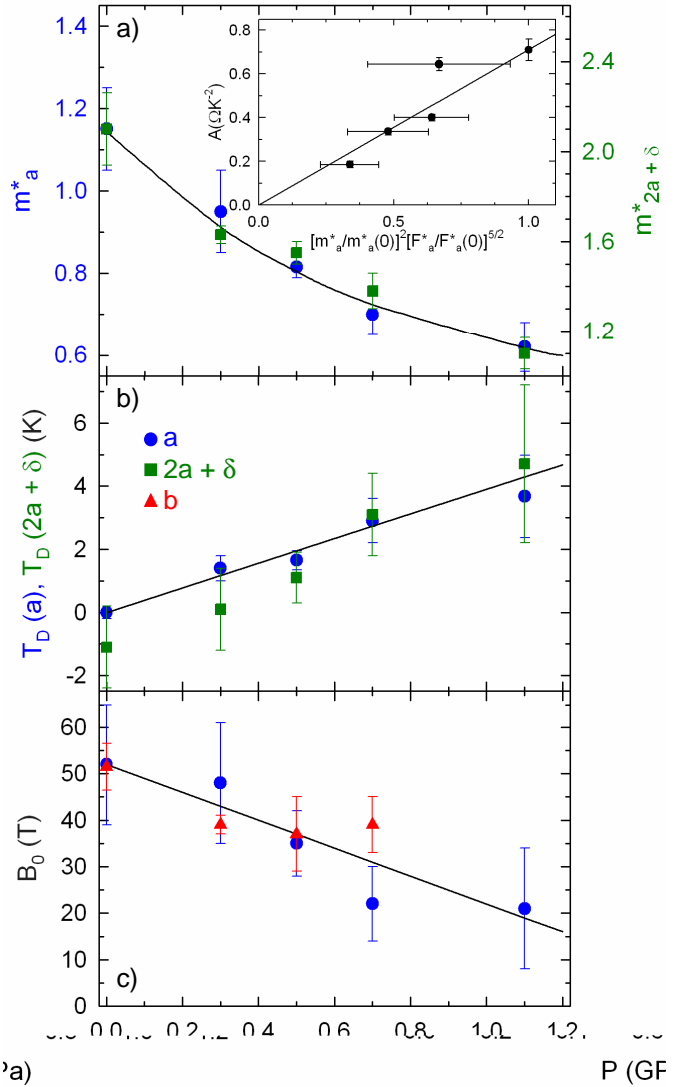


**Fig. 6.** Pressure dependence of the (a) effective mass, (b) Dingle temperature and (c) magnetic breakdown field, deduced from the field or temperature dependence of the Fourier components  $a$ ,  $2a + \delta$  and  $b$ . Lines are guides to the eye. The inset displays the  $A$  coefficient deduced from data in Fig. 2, plotted against  $[m_a^* / m_0^*]^2 / [F_a / F_0^*]^{5/2}$ , where  $m_0^*$  and  $F_0^*$  are the ambient pressure values. The straight line is the best fit of Eq. 4 to the data.

As displayed in Fig. 5,  $F_b$  (i. e. the FBZ area) linearly increases in the explored pressure range. The pressure sensitivity ( $d[F_b/F_b(P = 0.1 \text{ MPa})]/dP = 0.04 \text{ GPa}^{-1}$ ) is in good agreement with data of the FBZ area of numerous ET salts [30,31,32]. While the pressure dependence of  $F_a$  is the same as that of the FBZ area,  $F_\delta$  strongly decreases as the pressure increases. This behaviour, which lead to the non-monotonous pressure dependence of  $F_{2a+\delta}$  reported in the inset of Fig. 5, could be understood assuming that the long and small axis of the  $a$  orbits elongates and shrinks, respectively, as the pressure increases. However, although this is actually the case of the  $\beta$  orbits of  $\kappa$ -salts [30], such a behavior should lead to an increase of the  $\Delta$  piece area steeper than observed in Fig. 5. The actual scenario is therefore certainly more complex.

The MB field ( $B_0$ ), effective mass ( $m^*$ ) and Dingle temperature ( $T_D = \hbar/2\pi k_B \tau_D$ , where  $\tau_D$  is the relaxation time) can be extracted from the field and (or) temperature dependence of the oscillations amplitude. In the framework of the Lifshits-Kosevich model [2], the amplitude of the Fourier component with the frequency  $F_i$  is given by  $A_i \propto R_{Ti} R_{Di} R_{MBi} R_{Si}$ , where the spin damping factor ( $R_{Si}$ ) depends only on the direction of the magnetic field with respect to the conducting plane. The thermal (for a 2D FS), Dingle and MB damping factors are respectively given by:

$$R_{Ti} = \frac{\alpha T m_i^*}{B \sinh[\alpha T m_i^*/B]} \quad (1)$$

$$R_{Di} = \exp[-\alpha T_D m_i^*/B] \quad (2)$$

$$R_{MBi} = \exp\left(-\frac{t_i B_{MB}}{2B}\right) [1 - \exp(-\frac{B_{MB}}{B})]^{b_i/2} \quad (3)$$

where  $\alpha = 2\pi^2 m_e k_B / e \hbar$  ( $\simeq 14.69 \text{ T/K}$ ). Integers  $t_i$  and  $b_i$  are respectively the number of tunnelling and Bragg reflections encountered along the path of the quasiparticle.

As discussed in Refs. [11,12], only Fourier components  $a$ ,  $2a + \delta$  (SdH) and  $b$  (QI) can be analyzed on the basis of closed orbits or QI paths, the other being due to, or strongly affected by, the frequency mixing phenomenon. Therefore, we will mainly focus on these oscillations in the following.

In the field range below  $\sim 30 \text{ T}$ , the amplitude of the Fourier component linked to  $F_b$  remains temperature-independent up to 0.7 GPa (at 1.1 GPa, the signal-to-noise ratio is too small to derive a reliable temperature dependence). This feature is in agreement with the zero-effective mass value predicted for a symmetric quantum interferometer [33], as reported for ambient pressure data [11]. Oppositely,  $m^*(a)$  and  $m^*(2a + \delta)$  decreases by roughly a factor of 2 between ambient pressure and 1.1 GPa (see Fig. 6a). Remarkably, the ratio  $m^*(2a + \delta) / m^*(a)$  remains pressure-independent and equal to 1.8. This value is close to 2 as expected from the semiclassical model of Falicov-Stachowiak [1] for the considered coupled orbits networks [11]. The decrease of the effective mass as the applied pressure increases can be considered in the light of the  $T^2$  dependence of the zero-field resistance observed at low-temperature (see the inset of Fig. 2). Indeed, in the case of a strongly correlated Fermi liquid, the Kadowaki-Woods ratio ( $A / \gamma^2$ , where  $A$  and  $\gamma$  are the  $T^2$  coefficient of the resistivity and the electronic specific heat coefficient



cient, respectively) should be proportional to the lattice parameter [34]. Assuming, as a rough approximation, that  $\gamma \propto 1/\varepsilon_F \propto m^*(a) / F_a$  and, since the FBZ area varies as  $F_a$  under pressure, the relevant lattice parameter is proportional to  $1 / (F_a)^{1/2}$ , yield:

$$A \propto \left( \frac{m_a^*(P)}{m_a^*(P=0)} \right)^2 \left( \frac{F_a(P)}{F_a^*(P=0)} \right)^{5/2} \quad (4)$$

As can be observed in Fig. 6a, Eq. 4 accounts for the data within the error bars. Such a behaviour could suggest a reduction of electron correlations under pressure, in line with a Brinkman-Rice scenario [28]. However, it should be mentioned that the product  $A \times T_0^2$  (where  $T_0$  is the coherence temperature, above which the  $T^2$  law is no more valid) should be roughly pressure-independent within this picture which is not the case. Indeed, according to the data of Fig. 2, it decreases by about a factor of two from ambient pressure to 1.1 GPa which suggests that electron correlations may not be the only contribution to the observed behaviour. A similar conclusion is derived from the data of  $\kappa$ -(ET)<sub>2</sub>Cu[N(CN)<sub>2</sub>]Br [20].

Besides the effective mass, the two main ingredients entering the field dependence of the oscillation amplitude are the MB field and the Dingle temperature. Since the  $a$  orbits only involve Bragg reflections, both  $T_D$  and  $B_0$ <sup>2</sup> can be derived from this component [11,12]. The MB field value, consistently deduced from both the  $a$  and  $b$  components within the error bars, strongly decreases as the

applied pressure increases as reported in Fig. 6c. This behaviour is consistent with the data relevant to the MB orbit  $\beta$  reported for few charge transfer salts [30,31].  $T_D$  has been derived from the  $a$  and  $2a+\delta$  components, adopting the  $B_0$  value derived from  $a$  in the latter case (see Fig. 6b). As already reported [11], a slightly negative value is obtained at ambient pressure for  $2a + \delta$ . This can be due to a contribution of the frequency mixing phenomenon to this component. A lack of accuracy in the determination of  $B_0$  (large error bars are observed in Fig. 6c) can also contribute to this result since the  $2a + \delta$  orbits involves four tunnellings ( $t_{2a+\delta} = 4$  in Eq. 3) which makes the deduced  $T_D$  value very sensitive to  $B_0$ . A sizeable increase of the scattering rate, deduced from the field dependence of both the  $a$  and  $2a+\delta$  components, is observed under pressure. Indeed,  $T_D$  which is close to 0 at ambient pressure increases up to about 4 K at 1.1 GPa which corresponds to  $\tau_D = 0.3$  ps. Pressure-induced defects seems the most plausible explanation for this behaviour. However, it must be recalled that this high  $\tau_D$  value decreases back as the pressure is released which rules out any sample degradation due to the pressurization process. The increase of the scattering rate is in line with the pressure-induced resistance maximum observed in Fig. 2. However, as above discussed, the decrease of its amplitude above 0.5 GPa cannot be interpreted on this basis. An interplay between the pressure-induced decrease strength of the electron correlations and the increase of scattering rate, the latter being in this case assumed to be mainly controlled by electron-phonon interaction, could therefore be considered. Within

<sup>2</sup> Two different MB gaps are observed in Fig. 1. As discussed in Ref. [11], only a value very close to their arithmetic mean, can be derived from the field-dependent data.

this picture, it should also be assumed that the variations of the interlayer scattering rate, involved in the interlayer resistance, reflect that of the in-plane scattering rate which is probed by SdH oscillations. In any case, the observed pressure dependence of the Dingle temperature is at variance with the data of most ET-based salts for which  $T_D$  remains unchanged under pressure [31,35,36].

Finally, let us examine the pressure dependence of the frequency mixing that correspond to so called "forbidden orbits". They could arise from both chemical potential oscillation [3] and MB-induced Landau level broadening [4]. As mentioned in Ref. [13], applied pressure leads to an increase of the transverse interactions and therefore to a damping of the chemical potential oscillation. Oppositely, as can be observed in Fig. 4, the amplitude of some components such as  $\Delta + a$  or  $b + a$  remains large, or even increases, as the applied pressure increases. This behaviour suggests that the field-dependent chemical potential oscillation is not the dominant contribution to the development of the observed frequency combinations. This point is in line with recent calculations [37] which indicate that, contrary to the case of numerous ET salts which are uncompensated metals, chemical potential oscillation in compensated orbits systems is strongly damped. As a consequence, Landau level broadening is likely the main source of the observed frequency combinations in compensated orbits networks.

## 4 Summary and conclusion

The SdH spectra of the charge transfer salt  $(\text{ET})_8[\text{Hg}_4\text{Cl}_{12}(\text{C}_6\text{H}_5\text{Br})]_2$  exhibits many Fourier components corresponding to linear combinations of three basic frequencies ( $F_a$ ,  $F_\delta$  and  $F_\Delta$ ), in agreement with band structure calculations (see Fig. 1). Most of these frequency combinations, which correspond to "forbidden orbits" in the framework of the semiclassical model, keep a large amplitude in all the studied pressure range. This feature likely rules out chemical potential oscillation as a dominant contribution to their origin.

The pressure sensitivity of the FBZ area is similar to that of most of the ET salts. The area of the  $\Delta$  piece and of the compensated orbits ( $a$ ) follow the same pressure dependence as that of the FBZ area while the area of the  $\delta$  piece decreases under pressure. The measured electronic properties are significantly modified as the applied pressure increases. Either additional frequencies or shifts in few of the frequency combinations are observed in the high pressure range. Therefore, some change of the FS topology as the pressure increases cannot be excluded. Higher pressures are needed to check this hypothesis.

The zero-field interlayer resistance follows a  $T^2$  behaviour at low temperature with a pressure-dependent prefactor  $A$ , in agreement with the predictions for a strongly correlated Fermi liquid [34]. Since it strongly decreases under pressure, it could be inferred that the effect of electron correlations, which are important at ambient pressure decreases, under pressure. This latter point is in agreement with data relevant to e.g.  $\kappa$ -(ET) $_2$ Cu[N(CN) $_2$ ]Cl [22]. However, within this picture, the amplitude of the resistance

maximum should also continuously decrease as the applied pressure increases, which is not the case. Oppositely, it increases in the pressure range below about 0.5 GPa. In line with SdH data reported for  $\kappa\text{-(ET)}_2\text{Cu[N(CN)}_2\text{]Br}$  [23], the increase of the amplitude of the resistance maximum in the low pressure range could be attributed to the sizeable increase of the scattering rate, deduced from the SdH data, as the applied pressure increases. Within this picture, the pressure dependence of the interlayer resistance would mainly result from the interplay between the pressure sensitivity of the scattering rate and of the strength of electron-correlations.

This work was supported by Euromagnet under the European Union contract R113-CT-2004-506239, MEC-Spain (Project FIS2006-12117-C04-01, CSD2007-00041), Generalitat de Catalunya (Project 2005 SGR 683), the French-Russian exchange program between CNRS and RAS (number 21451) and by RFBR grants 09-02-00899 and 08-03-00480. We thank Jean-Yves Fortin, Sergei I. Pesotskii and Geert Rikken for interesting discussions.

## References

1. L. M. Falicov and H. Stachowiak, Phys. Rev. **147** 505 (1966).
2. D. Shoenberg, Magnetic Oscillations in Metals (Cambridge University Press, Cambridge, 1984).
3. A. S. Alexandrov and A. M. Bratkovsky, Phys. Rev. Lett. **76** 1308 (1996); Phys. Lett. A **234** 53 (1997) and Phys. Rev. B **63** 033105 (2001); T. Champel, *ibid.* **65** 153403 (2002); J. Y. Fortin, E. Perez and A. Audouard, *ibid.* **71** 155101 (2005).
4. A. B. Pippard, Proc. Roy. Soc. (London) **A270** 1 (1962); P. S. Sandhu, J. H. Kim and J. S. Brooks, Phys. Rev. B **56** 11566 (1997); J. Y. Fortin and T. Ziman, Phys. Rev. Lett. **80** 3117 (1998); V. M. Gvozdkov, Yu V. Pershin, E. Steep, A. G. M. Jansen and P. Wyder, Phys. Rev. B **65** 165102 (2002).
5. M.-H. Whangbo and E. Canadell, Acc. Chem. Res. **22** 375 (1989); M.-H. Whangbo, E. Canadell, P. Foury and J. P. Pouget, Science **252** 96 (1991).
6. U. Beierlein, C. Hess, J. Dumas, R. Buder, D. Groult, E. Steep, D. Vignolles and G. Bonfait. Eur. Phys. J. B **17** 215 (2000).
7. P. Foury-Leylekian, E. Sandré, S. Ravy, J.-P. Pouget, E. Elkaim, P. Roussel, D. Groult and Ph. Labbé, Phys. Rev. B **66** 75116 (2002).
8. S. Yasusuka, C. Terakura, T. Yakabe, Y. Terai, H. M. Yamamoto, R. Kato, S. Uji, Synth. Metals **135-136** 647 (2003); S. Yasusuka, S. Uji, K. Enomoto, T. Konoike, M. Nishimura, T. Terashima, D. Graf, E. S. Choi, J. S. Brooks, H. M. Yamamoto, R. Kato, K. Yokogawa and K. Murata, Synth. Metals **152** 437 (2005).
9. L. F. Veiros and E. Canadell, J. Phys. I France **4** 939 (1994).
10. C. Proust, A. Audouard, L. Brossard, S. I. Pesotskii, R. B. Lyubovskii and R. N. Lyubovskaia, Phys. Rev. B **65** 155106 (2002).
11. D. Vignolles, A. Audouard, L. Brossard, S. I. Pesotskii, R. B. Lyubovskii, M. Nardone, E. Haanappel and R. N. Lyubovskaya, Eur. Phys. J. B, **31** 53 (2003).
12. A. Audouard, D. Vignolles, E. Haanappel, I. Sheikin, R. B. Lyubovskii and R. N. Lyubovskaya, Europhys. Lett. **71** 783 (2005).
13. K. Kishigi and Y. Hasegawa, *ibid.* **65** 205405 (2002).

14. R. N. Lyubovskaia, O. A. Dyachenko, V. V. Gritsenko, Sh. G. Mkoyan, L. O. Atovmyan, R. B. Lyubovskii, V. N. Laukhin, A. V. Zvarykina and A. G. Khomenko, *Synth. Metals* **42** 1907 (1991).
15. M.-H. Whangbo and R. Hoffmann, *J. Am. Chem. Soc.* **100** 6093 (1978).
16. J. Ammeter, H.-B. Bürgi, J. Thibeault and R. Hoffmann, *J. Am. Chem. Soc.* **100** 3686 (1978).
17. M. Nardone, A. Audouard, D. Vignolles and L. Brossard, *Cryogenics* **41** 175 (2001).
18. D. Vignolles, V. N. Laukhin, A. Audouard, T. G. Prokhorova, E. B. Yagubskii and E. Canadell, *Eur. Phys. J. B* **51** 53 (2006).
19. R. B. Lyubovskii, S. I. Pesotskii and R. N. Lyubovskaya, *JETP Lett.* **62** 37 (1995), R. B. Lyubovskii, S. I. Pesotskii, A. Gilevski and R. N. Lyubovskaya, *J. Phys. I France* **6** 1809 (1996).
20. C. Strack, C. Akinici, V. Pashchenko, B. Wolf, E. Uhrig, W. Assmus, M. Lang, J. Schreuer, L. Wiehl, J. A. Schlueter, J. Wosnitza, D. Schweitzer, J. Muller and J. Wykhoff, *Phys. Rev. B* **72** 054511 (2005).
21. H. Urayama, H. Yamochi, G. Saito, K. Nozawa, T. Sugano, M. Kinoshita, S. Sato, K. Oshima, A. Kawamoto and J. Tanaka, *Chem. Lett.* 55 (1988); H. Müller, C.-P. Heidmann, A. Lerf, W. Biberacher, R. Sieburger and K. Andres, *Springer Proceedings in Physics*, Vol. 51, The Physics and Chemistry of Organic Superconductors, Springer-Verlag Berlin, Heidelberg 1990.
22. P. Limelette, P. Wzietek, S. Florens, A. Georges, T. A. Costi, C. Pasquier, D. Jérôme, C. Mézière and P. Batail, *Phys. Rev. Lett.* **91** 016401 (2003).
23. T. F. Stalcup, J. S. Brooks and R. C. Haddon, *Phys. Rev. B* **60** 9309 (1999).
24. J. G. Analytis, A. Ardavan, S. J. Blundell, R. L. Owen, E. F. Garman, C. Jeynes and B. J. Powell, *Phys. Rev. Lett.* **96** 177002 (2006).
25. T. Sasaki, N. Yoneyama, Y. Nakamura, N. Kobayashi, Y. Ikemoto, T. Moriwaki and H. Kimura, *Phys. Rev. Lett.* **101** 206403 (2008).
26. U. Lundin and R. H. McKenzie, *Phys. Rev. B* **68** 081101 (2003).
27. A. F. Ho and A. J. Schofield, *Phys. Rev. B* **71** 045101 (2005).
28. J. Merino and R. H. McKenzie, *Phys. Rev. B* **61** 7996 (2000).
29. Y. Maeno, K. Yoshida, H. Hashimoto, S. Nishizaki, S. Ikeda, M. Nohara, T. Fujita, A. P. Mackenzie, N. E. Hussey, J. G. Bednorz and F. Lichtenberg, *J. Phys. Soc. Jap.* **66** 1405 (1997).
30. J. Caulfield, W. Lubczynski, F. L. Pratt, J. Singleton, D. Y. K. Ko, W. Hayes, M. Kurmoo and P. Day, *J. Phys.: Condens. Matter* **6** 2911 (1994).
31. J. S. Brooks, X. Chen, S. J. Klepper, S. Valfells, G. J. Athas, Y. Tanaka, T. Kinoshita, N. Kinoshita, M. Tokumoto, H. Anzai and C. C. Agosta, *Phys. Rev. B* **52** 14457 (1995).
32. M.V. Kartsovnik, W. Biberacher, K. Andres and N.D. Kushch, *JETP Lett.* **62** 905 (1995) [*Pis'ma Zh. Éksp. Teor. Fiz.* **62** 890 (1995)].
33. R. W. Stark and C. B. Friedberg, *Phys. Rev. Lett.* **26** 556 (1971).
34. G. Moeller, Q. Si, G. Kotliar, M. Rozenberg and D. S. Fisher, *Phys. Rev. Lett.* **74** 2082 (1995); R. H. McKenzie, arXiv:cond-mat/9802198.

- 35. J. Hagel, J. Wosnitza, C. Pfeleiderer, J. A. Schlueter, J. Mohtasham and G. L. Gard, Phys. Rev. B **68** 104504 (2003).
- 36. D. Vignolles, A. Audouard, V. N. Laukhin, M. Nardone, E. Canadell, N. G. Spitsina and E. B. Yagubskii, Synth. Met. (2008), DOI: 10.1016/j.synthmet.2008.06.026
- 37. J. Y. Fortin and A. Audouard, Phys. Rev. B **77** 134440 (2008).